Calhoun
Institutional Archive of the Naval Postgraduate School

Calhoun: The NPS Institutional Archive

DSpace Repository

Theses and Dissertations | 1. Thesis and Dissertation Collection, all items

1989

Meandering of the coastal upwelling jet near Cape Mendocino

Fasciano, William Culp.

http://hdl.handle.net/10945/27126

This publication is a work of the U.S. Government as defined in Title 17, United States Code, Section 101. Copyright protection is not available for this work in the United States.

Downloaded from NPS Archive: Calhoun

http://www.nps.edu/library

Calhoun is the Naval Postgraduate School's public access digital repository for research materials and institutional publications created by the NPS community. Calhoun is named for Professor of Mathematics Guy K. Calhoun, NPS's first appointed -- and published -- scholarly author.

Dudley Knox Library / Naval Postgraduate School
411 Dyer Road / 1 University Circle
Monterey, California USA 93943

NAVAL POSTGRADUATE SCHOOL
Monterey, California

THESIS

F2372

MEANDERING OF THE COASTAL UPWELLING JET
NEAR CAPE MENDOCINO, CALIFORNIA:
A COMPARISON BETWEEN LABORATORY
SIMULATIONS AND OCEANIC OBSERVATIONS

by

William Culp Fasciano

June 1989

Thesis Advisor: Steven R. Ramp

Approved for public release; distribution is unlimited.

T244070

CARMEL, CALIFORNIA 93943-5002

SECURITY CLASSIFICATION OF THIS PAGE

REPORT DOCUMENTATION PAGE

Form Approved
OMB No. 0704-0188

1a REPORT SECURITY CLASSIFICATION UNCLASSIFIED	1b RESTRICTIVE MARKINGS None
2a SECURITY CLASSIFICATION AUTHORITY n/a	3 DISTRIBUTION/AVAILABILITY OF REPORT Approved for public release; distribution is unlimited
2b DECLASSIFICATION/DOWNGRADING SCHEDULE	
4 PERFORMING ORGANIZATION REPORT NUMBER(S)	5 MONITORING ORGANIZATION REPORT NUMBER(S)
6a NAME OF PERFORMING ORGANIZATION Naval Postgraduate School 6b OFFICE SYMBOL (If applicable) Code 68	7a NAME OF MONITORING ORGANIZATION Naval Postgraduate School
6c ADDRESS (City, State, and ZIP Code) Monterey, CA 93943-5000	7b ADDRESS (City, State, and ZIP Code) Monterey, CA 93943-5000
8a NAME OF FUNDING/SPONSORING ORGANIZATION 8b OFFICE SYMBOL (If applicable)	9 PROCUREMENT INSTRUMENT IDENTIFICATION NUMBER
8c ADDRESS (City, State, and ZIP Code)	10 SOURCE OF FUNDING NUMBERS PROGRAM ELEMENT NO / PROJECT NO / TASK NO / WORK UNIT ACCESSION NO

11 TITLE (Include Security Classification)
MEANDERING OF THE COASTAL UPWELLING JET NEAR CAPE MENDOCINO, CA: A COMPARISON BETWEEN LABORATORY SIMULATIONS AND OCEANIC OBSERVATIONS (UNCLASSIFIED)

12 PERSONAL AUTHOR(S)
Fasciano, William C.

13a TYPE OF REPORT	13b TIME COVERED	14 DATE OF REPORT (Year, Month, Day)	15 PAGE COUNT
Master's Thesis	FROM _____ TO _____	1989 June	68

16 SUPPLEMENTARY NOTATION The views expressed in this thesis are those of the author and do not reflect the official policy or position of the Department of Defense or the U.S. Government.

17 COSATI CODES			18 SUBJECT TERMS (Continue on reverse if necessary and identify by block number)
FIELD	GROUP	SUB-GROUP	Cape Mendocino, Upwelling, bottom topography, Laboratory models, Meandering coastal jet.

19 ABSTRACT (Continue on reverse if necessary and identify by block number)

The physics of a rotating tank laboratory model, developed by Narimousa and Maxworthy (1985) to simulate the dynamics of coastal upwelling, is tested by applying the model to real ocean data from shipboard surveys in the Coastal Transition Zone off central California. The primary goal is to test the hypothesis that flow over bottom topography, i.e., the Mendocino Ridge, is an important mechanism for generating the meandering structure of the coastal upwelling jet. More specifically, the goal is to test the model's ability to reproduce the offshore and alongshore meandering length scales observed from satellite imagery and maps of dynamic height.

Results show that the model incorrectly predicts the necessary conditions for eddy shedding in areas where this phenomenon is observed. The prediction criterion parameter (Θ_A) is not considered physically meaningful. Evidence is presented to show that the model significantly overestimates the Richardson number along with offshore and alongshore meandering length scales of the upwelling coastal jet. Some possible explanations for this are discussed.

20 DISTRIBUTION/AVAILABILITY OF ABSTRACT	21 ABSTRACT SECURITY CLASSIFICATION
☐ UNCLASSIFIED/UNLIMITED ☐ SAME AS RPT ☐ DTIC USERS	Unclassified
22a NAME OF RESPONSIBLE INDIVIDUAL Steven R. Ramp	22b TELEPHONE (Include Area Code) / 22c OFFICE SYMBOL Code 68Ra

DD Form 1473, JUN 86 *Previous editions are obsolete.* SECURITY CLASSIFICATION OF THIS PAGE

S/N 0102-LF-014-6603

Approved for public release; distribution is unlimited.

Meandering of the Coastal Upwelling Jet Near Cape Mendocino, California: A Comparison Between Laboratory Simulations and Oceanic Observations

by

William Culp Fasciano
Lieutenant Commander, United States Navy
B.A., Humboldt State University, 1971
M.S., John Carroll University, 1973

Submitted in partial fulfillment of the
requirements for the degree of

MASTER OF SCIENCE IN PHYSICAL OCEANOGRAPHY

from the

NAVAL POSTGRADUATE SCHOOL
June 1989

DUDLEY KNOX LIBRARY
NAVAL POSTGRADUATE SCHOOL
MONTEREY, CALIFORNIA 93943-5002

ABSTRACT

The physics of a rotating tank laboratory model, developed by Narimousa and Maxworthy (1985) to simulate the dynamics of coastal upwelling, is tested by applying the model to real ocean data from shipboard surveys in the Coastal Transition Zone off central California. The primary goal is to test the hypothesis that flow over bottom topography, i.e., the Mendocino Ridge, is an important mechanism for generating the meandering structure of the coastal upwelling jet. More specifically, the goal is to test the model's ability to reproduce the offshore and alongshore meandering length scales observed from satellite imagery and maps of dynamic height.

Results show that the model incorrectly predicts the necessary conditions for eddy shedding in areas where this phenomenon is observed. The prediction criterion parameter (θ_*) is not considered physically meaningful. Evidence is presented to show that the model significantly overestimates the Richardson number along with offshore and alongshore meandering length scales of the upwelling coastal jet. Some possible explanations for this are discussed.

C.1

TABLE OF CONTENTS

I. INTRODUCTION 1

II. THE MODEL 7

III. DATA 15

IV. RESULTS 26

V. DISCUSSION 40

VI. CONCLUSIONS AND RECOMMENDATIONS 47

APPENDIX - DERIVATION OF MODEL OUTPUT PARAMETERS . . . 49

LIST OF REFERENCES 52

INITIAL DISTRIBUTION LIST 57

LIST OF TABLES

TABLE 3.1 OBSERVED VALUES OF L_s, THE FINAL DISTANCE OF THE UPSTREAM FRONT FROM THE COAST. [FROM SATELLITE AVHRR SST IMAGERY OBTAINED DURING THE JUNE 1987 (NPS) CRUISE 21

TABLE 3.2 RELATIONSHIP OF MODEL PARAMETERS TO REAL OCEAN OBSERVATIONS 22

TABLE 4.1 MODEL INPUT AND OUTPUT PARAMETERS FOR REAL OCEAN OBSERVATIONS, COMPARED WITH THE PARAMETERS CALCULATED BY BOTH THE FRICTION VELOCITY AND VELOCITY SHEAR TECHNIQUES. STATIONS USED (MAY, STA. 97; JUNE STA. 89) ARE NEAR THE "JET." L_s = 90 KM 31

TABLE 4.2 EXTREME VALUES OF MODEL INPUT AND OUTPUT PARAMETERS TAKEN FROM TWO SECTIONS FROM THE JUNE 87 (NPS) CRUISE. SEE FIGURE 4.6 FOR STATION LOCATIONS. L_s = 90 KM 32

LIST OF FIGURES

Figure 2.1 Experimental tank apparatus. (a) Side view of the experimental apparatus. (b) Side view of the experimental tank with a cross-section at the ridge (measurements in cm). [From Narimousa and Maxworthy (1985).] 12

Figure 2.2 Streak photograph illustrating model parameters, L_s and L_n. The ridge extends from the center of the tank to the top of the photograph [From Narimousa and Maxworthy (1985).] 13

Figure 2.3 Streak photograph illustrating model parameter, D_{sw}. This illustrates the presence of the ridge and the scale of the downstream standing wave. Note the decrease in the amplitude of the waves downstream from the ridge. [From Narimousa and Maxworthy (1985).] 14

Figure 3.1 AVHRR satellite SST imagery, 10 June 1987. This is used to estimate values for L_s, L_n, and D_{sw}. [Provided by Scripps Institution of Oceanography.] 23

Figure 3.2 Map of dynamic height of the sea surface relative to 500 db for the May 1987 data. This shows measures for L_s, L_n, and D_{sw}. [From "OSU Data Report for CTD Observations in the Coastal Transition Zone Off Northern California, 18-26 May 1987."] 24

Figure 3.3 Map of dynamic height of the sea surface relative to 500 db for the June 1987 data. This shows the measurements for L_s, L_n, and D_{sw}. [From "OSU Data Report for CTD Observations in the Coastal Transition Zone Off Northern California, 9-18 June 1987."] 25

Figure 4.1 Cross section of sigma theta, May 87 (OSU) cruise, from which h_o and g' are measured to determine θ_o. [From "OSU Data Report for CTD Observations in the Coastal Transition Zone Off Northern California, 24-26 May 1987."]. 33

Figure 4.2 Cross section of sigma theta, June 87 (OSU) cruise, from which h_o and g' are measured to determine θ_o. [From "OSU Data Report for CTD Observations in the Coastal Transition Zone Off Northern California, 9-18 June 1987."] 34

Figure 4.3 Station locations, May 87 (OSU) Cruise. [From "OSU Data Report for CTD Observations in the Coastal Transition Zone Off Northern California, 18-26 May 1987."]. 35

Figure 4.4 Station Locations, June 87 (OSU) Cruise. [From "OSU Data Report for CTD Observations in the Coastal Transition Zone Off Northern California, 9-18 June 1987."] 36

Figure 4.5 Streak photograph illustrating the effect of decreasing θ_o, from 16.35 (top) to 6.43 (middle) to 2.57 (bottom). As θ_o decreases, the flow in the tank becomes qualitatively similar to that observed in the real ocean. [From Narimousa and Maxworthy (1985).] 37

Figure 4.6 Station locations, June 87 (NPS) cruise 38

Figure 4.7 Map of surface dynamic height, relative to 500 db, for the June 87 (NPS) cruise. 39

Figure A.1 Scatter plot showing how L_n, the distance of the head of the plume from the tank wall varies with time. (The solid dots represent θ_o 2.03 and the +'s represent θ_o = 36.43) [From Narimousa and Maxworthy (1985).] 50

Figure A.2 The bottom data represent variations of L_n/L_* for different values of θ_o. [From Narimousa and Maxworthy (1985).] 50

Figure A.3 The variation of D_{sw}/L_s (D_{sw} is the distance of the large standing wave from the maximum plume) with θ_o. [From Narimousa and Maxworthy (1985).] 51

I. INTRODUCTION

The California Current System (CCS) has been the subject of numerous research projects and extensive data collection efforts in the past decade. A basic description of the climatological California Current is presented by Hickey (1979). A basic component includes an equatorward mean flow which is driven by the wind stress over the Eastern North Pacific. This mean flow is difficult to observe but is clear in the dynamic topography (University of Hawaii, 1974), and has recently been confirmed using long term satellite drifters (Niiler and Brink, 1989). The observed currents off central California often resemble a complex eddy field (Reinecker *et al.*, 1987; Simpson *et al.*, 1986; Brink, 1983). Associated with this equatorward wind stress is the offshore surface Ekman drift during March through October, resulting in coastal upwelling. A geostrophically balanced equatorward jet flows along the upwelling front (Brink, 1983), which may develop meanders as the upwelling season progresses. The structure of the coastal jet is highly time variable and the strength and size strongly depends on the local winds (Winant *et al.*, 1987). Poleward flow has long been known to exist (Sverdrup *et al.*, 1942). This poleward flow has been observed at various depths and distances offshore. The complete dynamics of poleward flow is not well understood but distinct seasonal differences have been observed. In the winter, off the Oregon and California coasts, the predominant winds (the primary

forcing) are southeasterly which cause a shoreward Ekman transport and subsequent downwelling. In this regime there is a broad, near-shore, poleward, surface current (Davidson current), which extends from the coast to beyond the continental shelf with speeds ranging from 20 cm/s to 30 cm/s (Wyatt *et al.*, 1972; Reid *et al.*, 1962; Huyer, 1977; Chelton, 1984; Hickey, 1981; Strub *et al.*, 1987). The strongest flow occurs adjacent tc the coast, over the inner shelf (Huyer *et al.*, 1978). In the summer upwelling season, poleward surface currents are observed off central California. These poleward flows are confined to the region shoreward of the equatorward jet which flows along the front between the dense, freshly upwelled coastal waters and the less dense surface water. These inshore, poleward, flows still have considerable widths, up to 100 km or more (Reid *et al.*, 1962).

Over the shelf, a poleward undercurrent has been observed with its maximum strength within 20 to 30 m of the bottom (Huyer *et al.*, 1978). Compared to the Davidson current, these flows are weaker, 2 to 5 cm/s. This current seems to "disappear" coincident with the onset of upwelling in the spring (Lentz, 1987). Several weeks later, it "appears" again and gains strength throughout the summer regime (Lentz, 1987). In the fall the current maximum seems to shoal and merge with the Davidson current. Offshore from the shelf, poleward undercurrents are also observed (Tibby, 1941). This poleward flow (the California Undercurrent) is observed below 200 m from Baja California to north of Cape Mendocino, (Reid *et al.*, 1962). Several forcing mechanisms for

the California Undercurrent have been suggested: wind relaxation (Huyer and Kosro, 1987), remote forcing by the wind, and the steady state component of the wind stress curl (McCreary *et al.*, 1987). Thermohaline forcing may also be important for other eastern boundary currents (e.g., Leeuwin Current), but seems less important in the CCS.

The area which has become known as the "Coastal Transition Zone" (CTZ) has attracted much interest to increase the understanding of the effects of upwelling on changes in the chemistry and biology of the ocean. This region has been defined as the intermediate area from the shelf break to 200 km offshore, between the coastal waters and the open ocean where large energetic mesoscale eddies, cross-shore jets and cold filaments are observed (The CTZ Group, 1988). The primary research effort has been focused on the central California area bounded by Point St. George, OR and Point Conception, CA. The research goals of the CTZ program are to enhance the understanding of the kinematics and dynamics of the cold filaments (broad bands of cold water which can extend 100 to 300 km offshore), which are often observed in the satellite sea surface temperature (SST) imagery corrected by the Advanced Very High Resolution Radiometer (AVHRR). AVHRR and Coastal Zone Color Scanner (CZCS) imagery of the central California coast are used in conjunction with *in-situ* measurements to assess the impact of these structures on the cross-shelf transport and the biological productivity of the region. A primary objective is to study the spatial and temporal evolution of the physical and biological

structure of cold filaments observed off the California coast. To accomplish this objective, extensive field measurements of the relevant physical and biological parameters were made from research vessels and satellites at scales ranging from the microscale to the mesoscale. The data are presently being compared with numerical, assimilative and laboratory models. The CTZ program is described in further detail by Brink and Hartwig [Office of Naval Research (1986).] Strong evidence from the 1987 and 1988 field programs conducted by the Naval Postgraduate School and Oregon State University suggest that some form of a meandering upwelling jet may be at least partly responsible for the large cold filaments observed off the central California coast (Kosro *et al.*, in press).

Why does the upwelling jet meander? Several possible mechanisms have been suggested. The most often considered mechanisms are: baroclinic instability (Ikeda and Emery, 1984; Batteen, in press); bottom topography (Preller and O'Brien, 1980; Brink, 1987; Narimousa and Maxworthy, 1985); coastal irregularities (Peffly and O'Brien, 1976; Crepon *et al.*, 1984; Narimousa and Maxworthy, 1987); and wind stress (Allen, 1980; Batteen *et al.*, in press). Barth (1987) shows that when considering the energy balances involved, a complicated interaction can exist between the large-scale currents in the ocean and the synoptic scale eddies. In particular, a transfer of available potential energy can occur between the eddies and the large scale currents. An upwelling plume of cold water can account for the energy balance in the energy conservation process (Barth, 1987).

The general shape of the coastline (capes and headlands) may have an important bearing on both the initial formation of the upwelling jet and the subsequent meandering process. Crepon *et al.*, (1984) show that coastline structure has an effect on the formation of upwelling centers, i.e., areas of intensified coastal upwelling where the alongshore and offshore spatial scales are roughly comparable. However, after having considered several models and formulations for this effect (e.g., conservation of potential vorticity around a cape), Brink (1983) concludes, based on Peffley and O'Brien's (1976) numerical modeling results, that the coastline effect may be simply caused by the general correspondence of capes to submarine ridges and bays to submarine valleys so that coastline geometry likely plays a minor role, if any, in the initial formation of the jet. Narimousa and Maxworthy (1987) infer, by laboratory experiments, that coastline geometry can have an effect on the meandering process.

Flow over irregular bottom topography, particularly the Mendocino Ridge, may be important in initiating the meandering of the upwelling front. Narimousa and Maxworthy (1985), hereafter NM85, designed a rotating tank experiment to examine the flow of a two layer fluid near a ridge. One of their basic goals was to develop parameters that could be used to predict the possibility of instabilities and eddy shedding along with values for alongshore wavelengths of the meandering current (The full model will be described in more detail in the next section). A ridge placed along the bottom of the tank simulates a bottom structure such as the Mendocino Ridge. By performing different experiments

with and without the ridge in place, the NM85 model was able to make several conclusions concerning the effect of the ridge. The first sign of upwelling occurs near the ridge as a plume which moves offshore ahead of the upstream front to produce maximum upwelling near the downstream side of the ridge. Baroclinic waves form on the upwelling front in both cases. With the ridge in place, the dı ʕt velocity and the amplitude of the waves are reduced. As the waves approach the ridge, they become deformed and get absorbed by the jet on the ridge.

The basic objective of this thesis is to test the hypothesis that bottom topography, specifically the Mendocino Ridge, is important for generating the meandering structure of the coastal upwelling jet. More specifically, the goal is to use real ocean data with the physics ɔf the NM85 laboratory model to see if the model can correctly reproduce the meandering scales observed off central California.

II. THE MODEL

The NM85 laboratory model attempts to simulate the upwelling process when a wind stress is applied to the air-water interface of a two layer fluid. The effect of bottom topography is investigated by placing a ridge along the conical shaped bottom (Figure 2.1). The tank is filled with a saline solution and a second less dense solution is diffused on top of the heavier liquid with no appreciable mixing allowed. At the fluid interface, small neutrally buoyant particles are placed which allow streak photography to capture the motion of the fluid. Each run is initialized by starting the tank and allowing the fluid in both layers to come to solid body rotation.

A simulated wind stress is subsequently applied to the top surface by a counter rotating disk, which causes the interface to surface at the outermost edge of the tank. The sign of the stress is the same as that in eastern boundary currents in the real ocean. Due to the net forces acting on the fluids, the lighter fluid gives way and starts to migrate away from the wall. As this process continues, due to conservation of mass, the heavier fluid upwells from the bottom to replace the less dense fluid. When equilibrium is reached, there is a front established at a certain distance, L_s, from the wall, and the system is in geostrophic balance. Placing the ridge in the tank to simulate bottom topography causes the upwelled front to take on a much different appearance than is

observed without the ridge. Instabilities develop, and their dynamics are quite different on the upstream and downstream sides of the ridge. Upstream from the ridge a front develops and migrates away from the tank wall. The first indication of upwelling at the surface always occurs at the ridge in the form of a plume. Downstream from the ridge standing waves appear which decrease in amplitude with distance from the ridge. A short time later, baroclinic waves appear at the upstream front. These waves along with the front continue to migrate downstream. Subsequently, steady state is reached. Narimousa and Maxworthy (1985) present the details of these instabilities and note that in each of the eight experiments reported, baroclinic waves appeared at the upwelling front prior to the front achieving the steady state balance. For each of the eight experiments, the only parameters that varied were h_o, the initial depth of the less dense fluid, which ranged from 2.1 to 2.6 cm; the density difference between the layers, which ranged from 0.020 to 0.024 g/cm^3 and f, the Coriolis parameter, which ranged from 1.24 to 5.80 rad/s. The counter rotating disc rotation rate, $\Delta\Omega$, was kept constant at .0125 rad/s for each experiment. These eight experiments provided data points to establish empirically, the functional dependence between the model input and output parameters (see Appendix).

There are several non-dimensional parameters derived from the model, aside from the traditional Rossby radius of deformation, R_D, that could be used to compare the model output with real ocean data. The non-dimensional internal Rossby radius is given by: $R_D = (g'h_o)^{1/2}/fL_s$, (eqn. 2.1)

where L_* = the final distance of the upstream front from the wall; $g' = g\Delta\rho/\rho$ is the reduced gravity between the two layers; $f = 2\ \Omega$ is the Coriolis parameter (constant); and h_o is defined above. The disk friction velocity at the location of the upwelled front is u_*. The friction velocity of the water at the air-sea interface (u_*) is estimated from the experimentally determined functional dependence of u_* on the known velocity of the counter rotating disk and is approximately 1/10 the velocity of the rotating disk at the upwelling front. This approach allows u_* to be an independent parameter in the model.

The Richardson Number, used in the NM85 model to characterize the dynamics of coastal upwelling and the size and drift velocity of the baroclinic waves, was calculated using the relationship:

$$R_i = g'h_o/u_*^2 \qquad \text{(eqn. 2.2)}$$

(Note: The Richardson number can also be calculated using ocean stratification and velocity shear which will be shown in the next section.). The key input parameter used by the NM85 model was

$$\theta_* = g'h_o/u_*fL_* = (R_D)(R_i)^{1/2}. \qquad \text{(eqn. 2.3)}$$

This parameter, θ_*, is used in the NM85 model to determine 1) the instability of the baroclinic waves produced upstream from the ridge, 2) the size and drift velocity of the baroclinic waves and 3) the amplitude and wavelength of the standing waves that appear downstream from the ridge. NM85 investigates values of θ_* ranging from 2.03 to 26.77. These values of θ_* result from the extreme limits of the model input parameters that are varied, to obtain

from the extreme limits of the model input parameters that are varied, to obtain streak photographs, consistent with the physical design of the experimental apparatus. Values of $\theta_* < 2$ produced very large meanders and eddy shedding at the ridge, i.e., θ_* is a stability parameter of sorts which was used to classify the behavior of the fluid. The key parameter, θ_*, is directly proportional to the reduced gravity and initial depth of the less dense fluid and inversely proportional to the wind friction velocity, Coriolis parameter and the final distance of the upstream front from the wall. Therefore, increased stratification and upper layer depth cause θ_* to increase (more stable) while increased Coriolis parameter and surface wind stress cause θ_* to decrease (less stable).

The model output parameters are t_s, the time for the front to reach steady state a distance L_s from the wall; M_f, the migration rate of the front; L_n, the steady state distance of the head of the plume from the wall; and D_{sw}, the distance of the first downstream wave crest from the plume at the ridge. Figure 2.2 is a streak photograph showing where the parameters L_s and L_n are measured in the tank. Note that L_s is measured upstream from the ridge and L_n is on the ridge. Figure 2.3 illustrates the location of the first downstream standing wave. Note that the amplitude of the wave is substantially decreased from the wave on the ridge. As will be discussed later, suitable satellite imagery is not available to make conclusive statements concerning observed values for the migration rate of the front and the time for the front to reach steady state; therefore these latter two output parameters, L_n, D_{sw}, and the Richardson

number are the primary focus of attention in the remaining sections of this paper. These NM85 model output parameters are calculated using the empirical relationships derived from the model (see Appendix):

$$L_n = L_s\theta_*^{.25} \qquad \text{(eqn. 2.4)}$$

$$D_{sw} = 0.22\ L_s\theta_*^{1.15}. \qquad \text{(eqn. 2.5)}$$

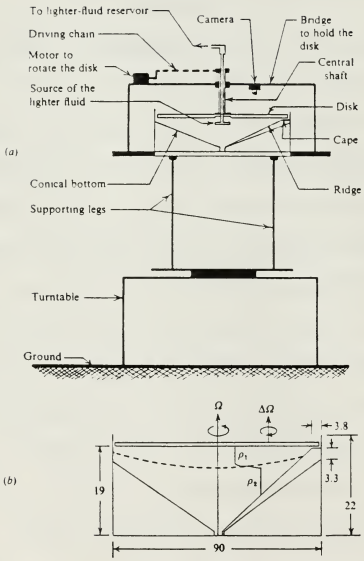

Figure 2.1 Experimental tank apparatus (a) Side view of the experimental apparatus. (b) Side view of the experimental tank with a cross-section at the ridge (measurements in cm). [From Narimousa and Maxworthy (1985).]

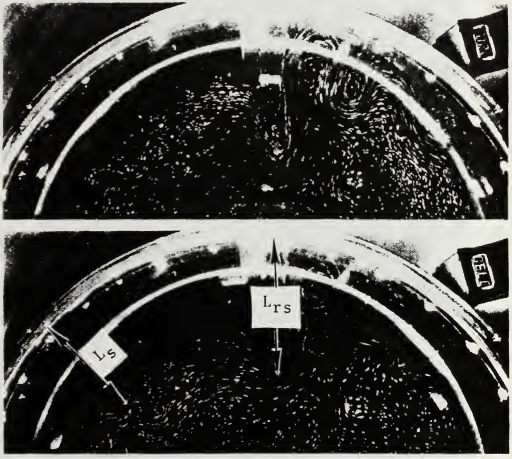

Figure 2.2 Streak photograph illustrating model parameters, L_s and L_{rs}. The ridge extends from the center of the tank to the top of the photograph [From Narimousa and Maxworthy (1985).]

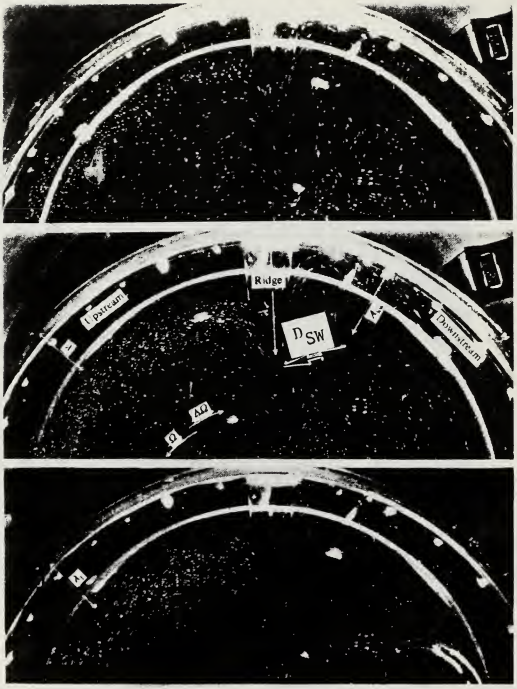

Figure 2.3 Streak photograph illustrating model parameter, D_{sw}. This illustrates the presence of the ridge and the scale of the downstream standing wave. Note the decrease in the amplitude of the waves downstream from the ridge. [From Narimousa and Maxworthy (1985).]

III. DATA

The *in-situ* data was collected on board the R/V PT. SUR in March and 9-18 June 1987, and on the R/V WECOMA in May and 15-28 June 1987 as part of the CTZ Program. The March, May and 9-18 June cruises mapped the transition zone between 38.0° N and 42.0° N using CTD, XBT and acoustic Doppler current profiler (ADCP) instrumentation along with continuous underway SST and salinity sensors. On the 15-28 June cruise, CTD, XBT and ADCP observations were made between 37.5° N and 39.5° N, using satellite SST measurements to track an upwelling filament using images received in real time. One hundred fifteen stations were completed with temperature, pressure, and salinity measured at one-meter intervals to five hundred meters depth.

Vertical and horizontal sections of temperature, salinity and geostrophic velocity were used with wind speed and direction at 10 m height to estimate the key input variables to the NM85 model (u_*, R_D, θ_* and R_I). In order to approximate the two-layer model in NM85, the depth of the maximum density gradient was calculated at each station. This depth, h_o, represents the depth of the boundary between the upper and lower portions of the ocean. The average density for each layer was also calculated along with the reduced gravity between the two layers.

Shipboard wind measurements were made continuously during all the cruises and averaged to hourly intervals. The alongshore component of the wind stress (τ) was calculated from the wind data using the relationship:

$$\tau = \rho_a C_D |u_{10}| v_{10} \qquad \text{(eqn. 3.1)}$$

where C_D = .0011 (Gill, 1982), ρ_a is the density of air, $|u_{10}|$ is the magnitude of the wind velocity observed at 10 meter height, and v_1 is its alongshore component. The wind stress values were averaged over the 2-3 days spent in the area. The friction velocity in the upper layer (u_*) was then calculated using the formulation:

$$u_* = (\tau/\rho_w)^{1/2} \qquad \text{(eqn. 3.2)}$$

where ρ_w is the density of the surface layer of the ocean (Kantha et al., 1977). Other estimates of the wind field were also compared using archived data from surface wind analyses produced by Fleet Numerical Oceanography Center (FNOC), Monterey, CA . Each source of wind field data examined produced the same general values for the local winds. The average alongshore vector averaged winds for the May and June (OSU) stations near the jet were 7.45 and 8.20 m/s, respectively. The May data were averaged over 2.6 days and the June data were averaged over 3.3 days. The vector averaged value of the alongshore component from archived FNOC data for the same time period and the same location was in close agreement, 8.36 m/s. The winds measured at 10 meters above the air-sea interface agree with typical values historically found in the same geographical area during the summer season (U.S. Department of

Commerce, 1977). Although the values used in the NM85 experiments were generated in a laboratory setting and were obviously known to a much higher accuracy because of the controlled nature of the experiment, the real ocean values used from shipboard measurements are considered to be representative of the seasonal wind field off California.

The most difficult of the input parameters to estimate from the data is L_s, the final distance of the upstream front from the coast as it impinges on the ridge. With the model, this distance is quite easily measured directly from the streak photograph. However, when trying to estimate this parameter with actual data, a difficulty arises when available AVHRR satellite imagery is examined to determine the parameter. The difficulty is determining exactly where and when the upwelling front is established in an AVHRR image. Figure 3.1 shows a AVHRR satellite photograph of the CTZ for June 10, 1987. Figures 3.2 and 3.3 show the dynamic topography for May 1987 and June 1987, respectively, used to "capture" the meandering scales. Kelly (1985) demonstrates based on data from Olivera, *et al.*, (1982) that in this geographic location (the CTZ), where density is a strong function of temperature maps of dynamic height closely resemble infrared satellite images. Figure 3.3 shows the surface dynamic topography relative to 500 dbar for a time period that overlaps that of the image, plotted on the same scale. There is a good correlation between the location of the jet in the dynamic topography and the position of the strong thermal gradient in the image separating the cold, upwelled water from the warmer offshore

water. This was also true of other image vs. *in-situ* comparisons made during the CTZ program. Knowing this, the position of the thermal front in other imagery can be used as a proxy for the location of the equatorward jet. The results (Table 3.1) using images close in time show a mean value of 92 +/- 10 km for L_s during early June 1987.

How do the laboratory tank parameters relate to the parameters measured for the real ocean? Table 3.2 shows how each of the key model input parameters relates to real ocean data. The final distance of the front from the wall of the tank, L_s, is analogous to the distance of the inshore edge of the upwelling front from the coast north of Cape Mendocino, when the flow is well developed and impinges on the ridge. This distance is estimated by measuring the distance from the coast to the point where the front is most pronounced on the satellite images or the maps of dynamic height. The reduced gravity, g′, in the model is easily calculated using the known fluid densities. For the ocean data, the depth of the maximum density gradient of the seasonal pycnocline for each station was determined; subsequently average densities were determined for a depth halfway between the surface and the depth of the maximum gradient and an equal depth below the depth of the maximum density gradient. In the model, h_o is easily measured as the initial depth of the less dense fluid. For the ocean, the depth of the maximum density gradient of the seasonal pycnocline, as discussed above, is used to estimate h_o. The model uses a constant value for the Coriolis parameter, f, based on the rotation rate of the tank. In the ocean this

value varies with latitude. This key difference may be important in determining the amplitude structure of the downstream standing waves. The friction velocity, u_*, is constant in the model. For the real ocean, actual winds are variable in space and time which in turn cause u_* to vary in space and time.

As described in the previous section, the Richardson number was calculated by NM85 using equation 2.1. The alternative definition of R_i is based on the Brunt-Väisälä frequency and the vertical velocity gradient:

$$R_i = N^2/(dv/dz)^2, \qquad \text{(eqn. 3.3)}$$

where N is the Brunt-Väisälä frequency and dv/dz is the vertical velocity shear. For this method, the geostrophic velocity is calculated for each pair of stations using dynamic heights provided in the OSU data reports. The geostrophic velocity (referenced to 500 db), V_g, is given by:

$$V_g = (10/fL)(D_B - D_A) \qquad \text{(eqn. 3.4)}$$

where L is the distance between the stations, D_A and D_B are dynamic heights at station A and station B and f is the Coriolis parameter. A "bulk" Richardson number was calculated by considering the velocity shear, based on geostrophic velocities, using vertical sections of density and geostrophic velocity and applying Equation 3.3 at each station.

The NM85 output parameters that this study focuses on are the steady state distance of the head of the plume from the coast, L_n, and the distance of the first downstream wave crest from the plume at the ridge, D_{sw}, because these can be most accurately determined from the real ocean data available. The two

meandering length scales were measured using maps of dynamic height of the sea surface relative to 500 db as shown in Figures 3.2 and 3.3. These values are analogous to the NM85 model parameters calculated using the empirical relationships derived from the model, Equations 2.4 and 2.5. The NM85 output parameter, M_f, the migration rate of the front, was not estimated nor compared with real ocean data in this paper because the time series of satellite imagery was insufficient to obtain the time rates of change needed for meaningful results.

TABLE 3.1 OBSERVED VALUES OF L_s, THE FINAL DISTANCE OF THE UPSTREAM FRONT FROM THE COAST. [FROM SATELLITE AVHRR SST IMAGERY OBTAINED DURING THE JUNE 1987 (NPS) CRUISE.]

Date (1987)	L_s (km)
10 June	100
16 June	74 - 92
21 June	96
22 June	84 - 92
23 June	87 - 107

TABLE 3.2 RELATIONSHIP OF NM85 MODEL PARAMETERS TO REAL OCEAN OBSERVATIONS.

Parameter	Model	Ocean
L_s	Measured from the tank wall	Estimated from satellite imagery & maps of dynamic height
g'	Calculated from known fluid densities	Estimated by finding the maximum density gradient of the seasonal pycnocline to divide the ocean into two layers
h_o	Measured depth of the dense fluid	Depth of the maximum gradient of seasonal pycnocline
f	Constant, based on the rotation rate of the tank	Varies with latitude
u_*	Determined empirically so that u_* can be used as an independent variable ($u_* = {}^1/_{10}$ Plate velocity)	Determined from ship-board wind data

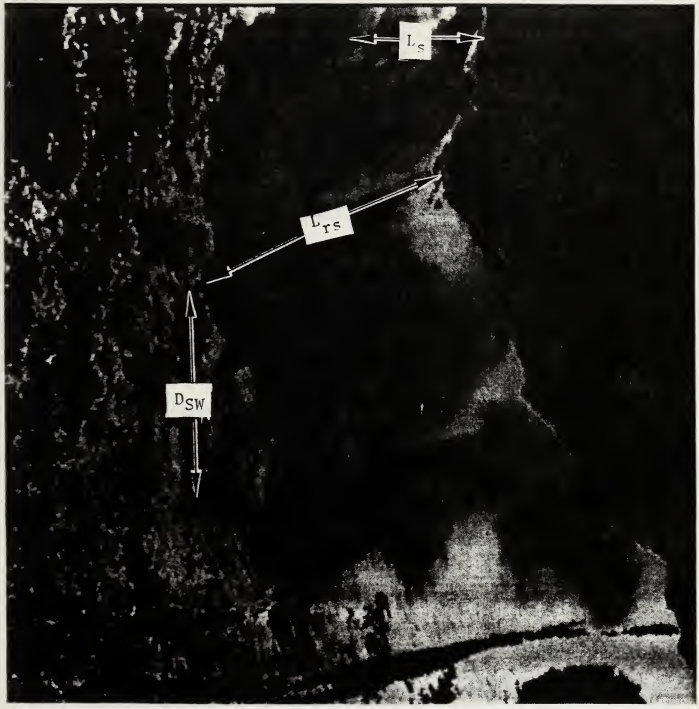

Figure 3.1 AVHRR satellite imagery, 10 June 1987. This is used to estimate values for L_s, L_{rs}, and D_{sw}. [Provided by Scripps Institution of Oceanography.]

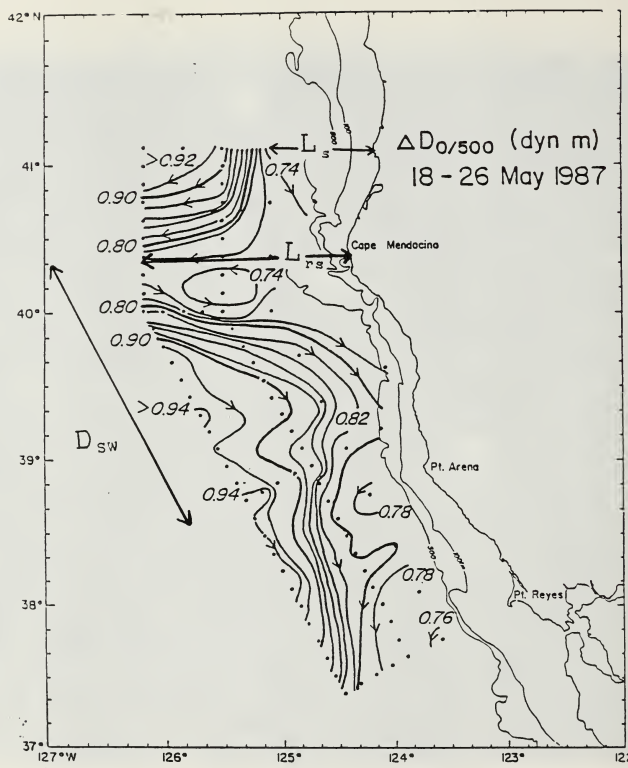

Figure 3.2 Map of dynamic height of the sea surface relative to 500db for the May 1987 data. This shows measures for L_s, L_{rs}, and D_{sw}. [From "OSU Data Report for CTD Observations in the Coastal Transition Zone Off Northern California, 18-26 May 1987".]

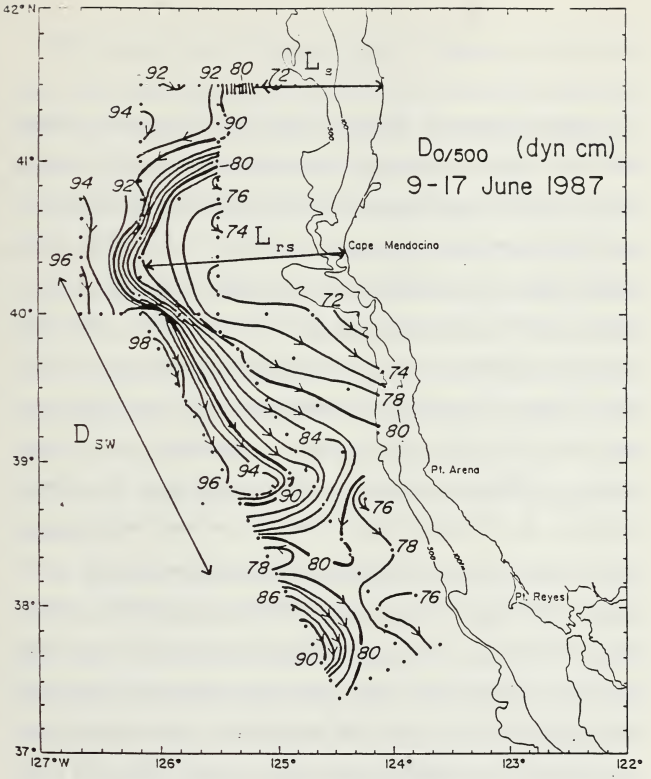

Figure 3.3 Map of dynamic height of the sea surface relative to 500 db for the June 1987 data. This shows the measurements for L_s, L_{rs}, and D_{sw}. [From "OSU Data Report for CTD Observations in the Coastal Transition Zone Off Northern California, 9-18 June 1987".]

In order to estimate the Richardson number (R_i) it is necessary to estimate the velocity difference (Δu) between the upper and lower layers of the fluid. In the tank experiments, this difference was ascribed entirely to the friction velocity u_*, estimated approximately as $u_* = 0.1\ U$, where U is the velocity of the counter-rotating plate. The Richardson number was then calculated as $g'h_o/u_*^2$ where h_o was the upper layer depth, and g' reduced gravity. This same information can likewise be used to estimate u_* in the ocean using $u_* = (\tau/\rho_w)^{1/2}$ (Eqn 3.2) where τ is the surface wind stress and ρ_w is the mean density in the upper layer of the water. This was done for consistency with the model, however, the Richardson number was also calculated using the traditional formulation, $R_i = N^2/(dv/dz)^2$ (eqn 3.3) where N is the Brunt-Väisälä frequency and the vertical shear was estimated across the main thermocline in the vicinity of the upwelling front, using the *in-situ* CTD data and geostrophic velocities from the CTZ program. This is a more accurate assessment of the actual shear between the upper and lower ocean. The typical observed mixed layer depth was in the 30-50 m depth range, while the estimation of the upper layer depth to the center of the thermocline for this data is of order 100 m. The strong shear across the main thermocline is clearly not directly wind driven, but appears instead to be due to baroclinic adjustment along the upwelling front (Kosro and Huyer, 1986).

The results are shown in Table 4.1. Table 4.1 summarizes the real ocean values observed and calculated from the May (OSU), and June (OSU) cruise data which are used for comparison with the NM85 model outputs, using both methods to calculate the shear between the upper and lower layer.

For the June 1987 time frame, a representative value for L_s is 92 +/- 10 km. Figures 3.2 and 3.3, maps of the dynamic height relative to 500 db, show L_s to be 83 and 93 km, respectively, and the mean value taken from satellite imagery (Table 3.1) is 92 km. The upper layer depth, h_o, used in calculating R_D and θ_* is defined here as the depth to the center of the seasonal pycnocline. The reduced gravity, g′, is defined by: $g' = g\Delta\rho/\rho$ using average values for the density in each layer. Values of g′ are used to determine R_D and θ_*. Values of g′, R_D and R_i are analyzed for each station and each of the model parameters is determined.

For purposes of illustration, two representative sections (Figures 4.1 and 4.2) from the May and June (OSU) cruises are used to compare NM85 model output results with the observed ocean parameters. For both pairs of stations (see Figures 4.3 and 4.4 for station locations), R_i is calculated using Equation 2.2 based on the surface wind stress and θ_* is calculated using Equation 2.3. Table 4.1 summarizes the NM85 input and output results. The observed values for L_n and D_{sw} from Figures 3.2 and 3.3 are also summarized in Table 4.1. Comparing the values in Table 4.1 shows that the NM85 model output using u_* slightly overestimates the offshore meandering length scale (L_n) and significantly

overestimates the alongshore meandering length scale (D_{sw}) by a factor of 2.5. As previously mentioned, R_i can also be calculated based on velocity shears, as shown in Equation 3.2. This method was also employed to see if using a Richardson number based on velocity shear would significantly affect the output results. The model output using dv/dz slightly underestimates both D_{sw} (by a factor of 2) and L_n.

In the NM85 model, L_n and D_{sw} are non-dimensionalized by dividing by L_s to make comparisons easier. For the real ocean, Table 4.1 shows an representative value for L_n = 165 km and D_{sw} = 250 km. Using an average L_s = 90 km, the ratios L_n/L_s and D_{sw}/L_s are 1.8 and 2.7 respectively. Table 4.1 shows that NM85 results show good agreement for the offshore ratio but an overestimation for the alongshore ratio by a factor of order 2.5.

The mean values for the internal Rossby radius for the May and June (OSU) data are 16 and 20 km for stations near the upwelling coastal jet. The average for the June (NPS) data is 7.7 km, considering each of the stations (7-11) in the jet (Figures 4.6 and 4.7). These values are in close agreement (within one standard deviation) with the 10 - 15 km estimates (Huyer, 1983) for mid-shelf regions located between 34° 45′ N and 43° 20′ N based on hydrographic sections made across the shelf region (Fleischbein *et al.*, 1981).

The resulting R_i values using the friction velocity technique are extremely large (order 15,000 to 20,000), and while they do ultimately produce reasonable values of the non-dimensional parameter θ_*, they do not seem to have any real

physical meaning in their own right other than to say that the water column is very stable vertically. The resulting values of θ_* were order 20 for the friction velocity technique and order 3 for the shear technique. Since the observed shear more accurately portrays the velocity difference between the upper and lower layer of the ocean, values of θ_* near 3 are likely more representative of the actual situation off Cape Mendocino.

Figure 4.5 is a streak photograph showing the upwelling plume occurring at the ridge in the tank. Figure 4.5 shows that, as θ_* becomes progressively smaller, the general character of the flow in the tank qualitatively approaches that observed in the real ocean. An important difference is that the meander amplitude in the tank decreases downstream, while the amplitude increases off central California (Kosro and Huyer, 1986; Niiler and Brink, 1989). Laboratory results predict that "pinched-off" cyclones will appear for θ_* less than 2. A strictly wind driven oceanic shear flow (θ_* = 17-21) would clearly not produce eddy shedding at the ridge. When the most realistic formulation for the shear between the upper and lower layer in the ocean was used (du/dz observed), the oceanic value of θ_* was about 3. While still "stable" this is very close to 2 and indicates that, given the approximations involved in our method, pinched off cyclones could potentially occur near the Mendocino Ridge, if the model physics applies. There is some observational evidence that pinched-off cyclones do occur off Mendocino. The June picture (Figure 3.3) could have resulted from the May picture (Figure 3.2) if either the upwelling front underwent a relaxation or if a

pinched-off cyclone occurred. Inspection of the AVHRR imagery archive (Kosro and Huyer (1986) Fig. 1; unpublished CTZ 88 data) also shows features that resemble pinched-off cyclones near Mendocino.

Table 4.1 shows that the NM85 model, using the wind stress formulation for calculating θ_*, predicts a very "stable", non-eddy shedding water column near Cape Mendocino. The time data (g' and h_o) input into the NM85 model using the alternative velocity shear formulation produces values of θ_* that are marginally "stable", but within the limits of experimental error reasonably imply the possibility of eddy shedding.

To test the representativeness of their results, the values of g', h_o, R_D, R_i, and θ_* were calculated for two sections across a meander observed during the June 15-28 cruise (Figures 4.6 and 4.7). These data were collected downstream of Cape Mendocino but give some idea of the range of values to be expected in both offshore and onshore sections of the Mendocino upwelling jet. For sections in the jet, θ_* values varied between 0.18 to 3.5 (Table 4.2) but were generally less than 2. This is consistent with the idea that eddy shedding is possible when realistic values of the shear across the thermocline are used for the calculation.

TABLE 4.1 MODEL INPUT AND OUTPUT PARAMETERS FOR REAL OCEAN OBSERVATIONS COMPARED WITH THE PARAMETERS CALCULATED BY BOTH THE FRICTION VELOCITY AND VELOCITY SHEAR TECHNIQUES. STATIONS USED (MAY, STA. 97; JUNE STA. 89) ARE NEAR THE "JET". L_s = 90 KM.

		g' m/s^2	h_0 m	τ $dynes/cm^2$	u $cm/_s$	$\frac{dv}{dz}$ $^1/_s \times 10^{-4}$	R_D	R_i	θ	N^2 $^1/_s \times 10^{-4}$	L_{rc} km	D_{sw} km	L_{rs}/L_s	D_{sw}/L_s
Observed	May	-	120	.808	.888	-	-	-	-	-	166	204	1.8	2.5
Observed	June	-	110	.965	.970	-	-	-	-	-	163	250	1.8	2.7
Friction Velocity Meth	May	.013	120	.808	.888	-	.147	20400	21	-	193	658	2.1	7.3
Friction Velocity Meth	June	.013	110	.965	.970	-	.138	15300	17	-	183	518	2.0	5.8
Velocity Shear Method	May	.013	120	-	-	4.26	.147	681	3.8	1.24	126	93	1.4	1.0
Velocity Shear Method	June	.013	110	-	-	6.81	.138	267	2.3	1.23	110	50	1.2	.56

TABLE 4.2 EXTREME VALUES FOR THE NM85 INPUT AND OUTPUT PARAMETERS TAKEN OVER THE ENTIRE SAMPLE SPACE FOR THE JUNE 87 (NPS) CRUISE. SEE FIGURE 4.6 FOR STATION LOCATIONS. L_s = 90 KM.

PARAMETER	MAXIMUM / STA	MINIMUM / STA
u_* (cm/s)	1.6/10	0.99/38
R_D	0.19/35	0.051/7
R_i	5448/35	12/8
θ_*	12/35	0.18/7
L_{rs} (km)	167/35	58.7/7
$D_{s,w}$ (km)	344/35	2.8/7

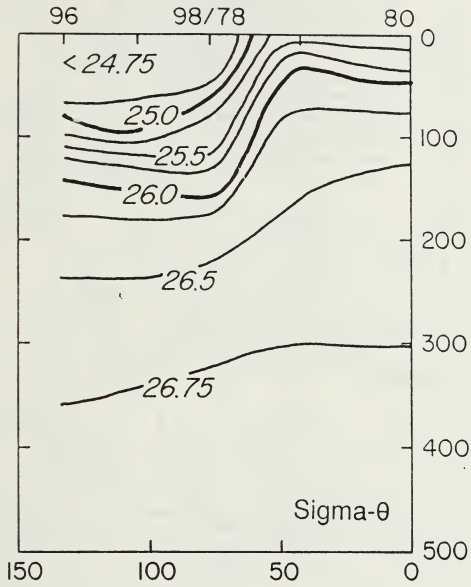

Distance (km) (along 41.1°N)

Figure 4.1 Cross section of sigma theta, May 87 (OSU) cruise, from which h_o, and g' are measured to determine θ_o. [From "OSU Data Report for CTD Observations in the Coastal Transition Zone OffNorthern California, 24-26 May 1987".]

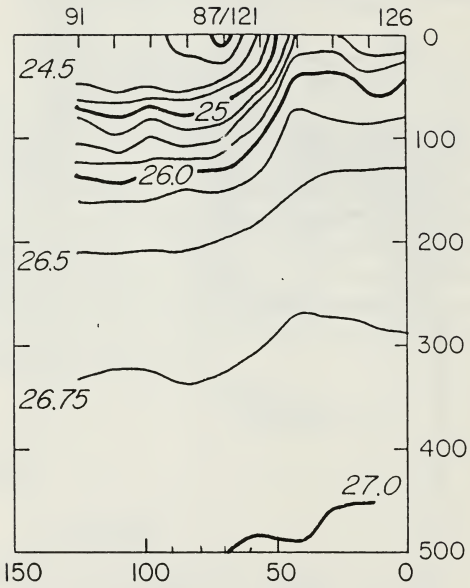

Figure 4.2 Cross section of sigma theta, June 87 (OSU) cruise, from which h_o, and g' are measured to determine θ_o. [From "OSU Data Report for CTD Observations in the Coastal Transition Zone Off Northern California, 9-18 June 1987".]

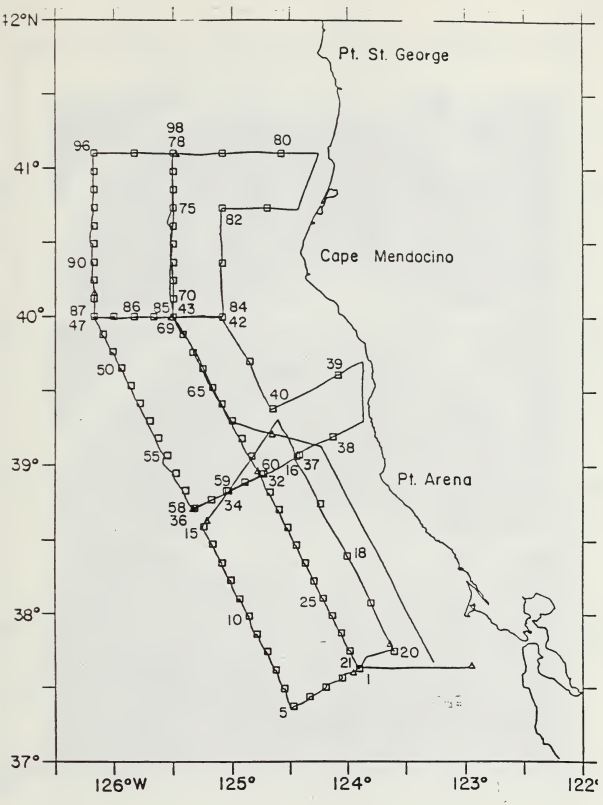

Figure 4.3 Station locations, May 87 (OSU) cruise. [From "OSU Data Report for CTD Observations in the Coastal Transition Zone Off Northern California, 18-26 May 1987".]

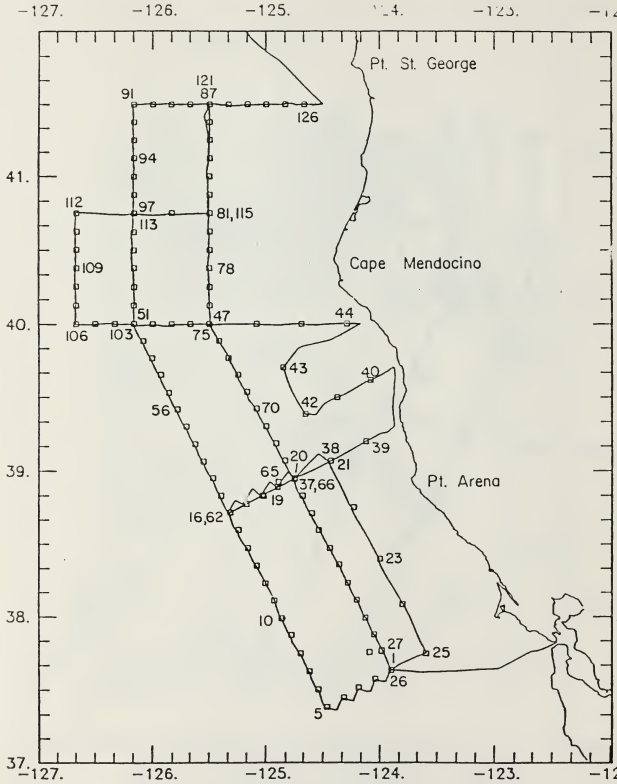

Figure 4.4 Station locations, June 87 (OSU) cruise. [From "OSU Data Report for CTD Observations in the Coastal Transition Zone Off Northern California, 9-18 June 1987".]

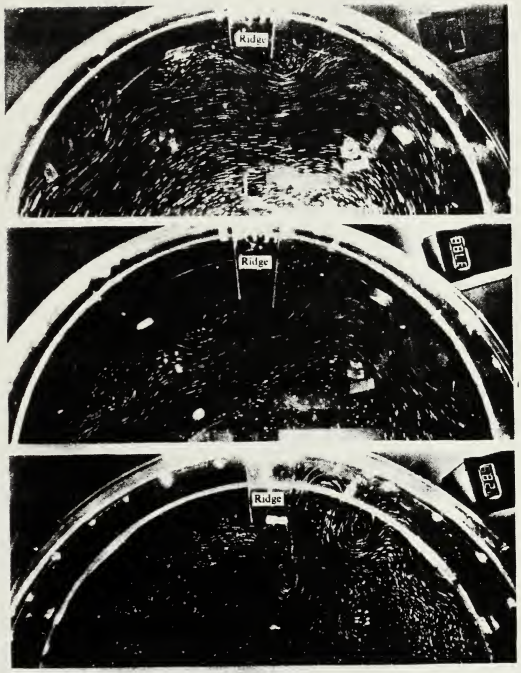

Figure 4.5 Streak photograph illustrating effect of decreasing θ_*. (From 16.35 (top) to 6.43 (middle) to 2.57 (bottom). As θ_* decreases, the flow in the tank becomes qualitatively similar to that observed in the real ocean.)[From Narimousa and Maxworthy (1985).]

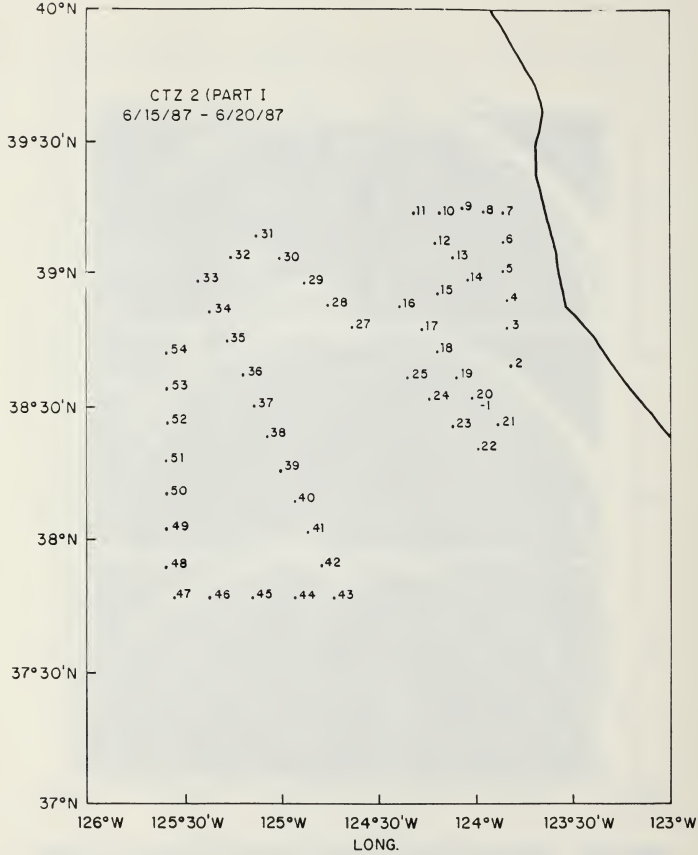

Figure 4.6 Station locations, June 87 (NPS) cruise.

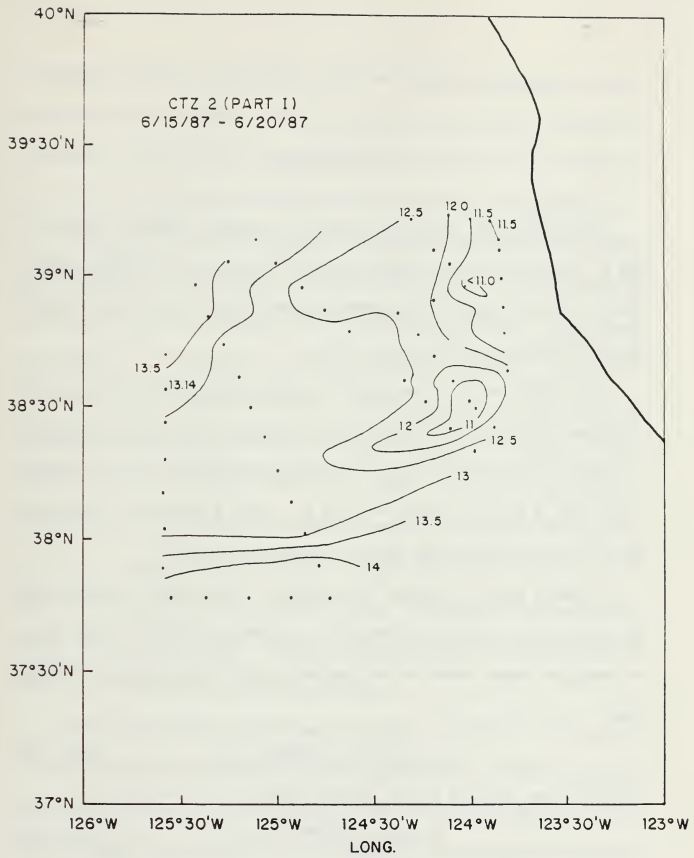

Figure 4.7 Map of dynamic height, relative to 500 db, for the June 87 (NPS) cruise.

V. DISCUSSION

The NM85 model uses the parameter θ_* to predict conditions which could lead to meandering currents and/or pinched-off eddies in an upwelling regime. NM85 concluded based on their experiments that values of θ_* less than 2 should allow eddy shedding at the ridge to occur.

The NM85 results do not correctly predict the observed values for the alongshore wavelength of the meandering current, D_{sw}. The NM85 model (using the friction velocity method) also overestimates the offshore steady state distance of the head of the plume from the coast L_n. These parameters are inherently tied to θ_* by the relationships given in equations 3.4 and 3.5.

It makes sense to examine the sensitivity of the results to each of the parameters (g',h_o, u_* and f) in equation 2.3. Assuming a value of 90 km for L_s, and using an average value for the observed L_n of 165 km, equation 3.4 shows that:

$$\theta_* = L_n^4/L_s^4 = 165^4/90^4 = 11.3. \qquad \text{(eqn. 5.1)}$$

For an average value for D_{sw} of 225 km, equation 3.5 shows that:

$$\theta_* = D_{sw}^{.87}/(.22^{.87}L_s^{.87}) = 8.2. \qquad \text{(eqn. 5.2)}$$

Using observed values for the meandering wavelengths in equations 3.3 and 3.4, derived from the NM85 model, θ_* needs to be order 10 in order for the model

to produce the correct wavelengths. This lies somewhere between the values calculated using the friction velocity and observed shear method. As Table 4.1 illustrates, the lowest values of θ_* calculated using equation 2.3 yield values for θ_* of order 20. There is little doubt that the model fails in this respect.

In addition to the overestimation of alongshore and offshore meandering scales, Figure 4.1 shows that in the tank, the amplitude of the meandering upwelling front tends to decrease in the downstream direction. In the ocean, specifically the CTZ (Figure 3.1), the trend is for the amplitude of the meander to increase in the downstream direction. This inconsistency may be due to the variation of the Coriolis parameter, f, in the ocean versus the constant f in the tank, i.e., there is no planetary β-effect in the tank. As f decreases equatorward, the long Rossby wave westward propagation speed βR_D^2 increases, which makes it easier for energy to propagate offshore. This is likely a small effect over 2.5° latitude, but does not exist at all in the tank. Alternatively, the ridge could simply act as a perturbation. Then the waves could grow downstream due to baroclinic instability (Watts and Johns, 1982).

Another aspect of the model that is not clear is the lack of incorporation of the ridge geometry and physics into the formulation for θ_*. It seems intuitive and certainly reasonable that the physics of the ridge should contribute to the dynamic instability and subsequent eddy shedding in a relatively shallow coastal ocean. The model, although possessing a ridge, does not show the functional dependence of θ_* on the relative ridge height and width with respect to ocean

depth or distance alongshore or offshore. The ridge geometry of the model varies somewhat from the bottom topography at the Mendocino Ridge. The ridge height at the highest point off Mendocino is on the order of 1100 m in 3700 m of water, a ratio of 0.30. In the tank, this ratio was 0.8, i.e., the ridge was considerably more pronounced in the tank, which should cause a greater perturbation of the flow than actually occurs in nature. The ridge width off Mendocino is on the order of 15 km, the same order of magnitude as the internal Rossby radius. In the tank, the ridge width (7.6 cm) is also about the same as the internal Rossby radius (8.7 cm). The flow should be able to "feel" the ridge in both cases. The ratio of ridge length to the maximum width of the ridge is 5.9 for the model and 4.6 for the Mendocino Ridge. There is no significant difference in this aspect of the geometry. Another significant comparison is the slope of the bottom from the coast out to the end of the ridge. For the model, this is relatively steep, 0.27, compared with 0.01 for the ocean floor near Mendocino. This large difference could have a significant impact on the relative importance of rotation vs. topography in the tank vs. the real ocean. The overall effect of these differences is not well understood, but the salient point is that this geometry is not incorporated into the θ_* formulation.

Some aspects of the model could not be investigated in this study. In particular, the model formulates a prediction for the speed of the upwelling front as it moves offshore. For the area of investigation, there is insufficient data to substantiate the correlation between the model output and observations. A

synoptic sequence of clear satellite imagery over a long enough time period (on the order of a week or two) is needed to accurately track the migration rate of the front.

The model results and observations in general do not agree. Possible explanations for this include: the variation of the Coriolis parameter with latitude, the spatial variation in surface wind stress, the importance of stratification, and the fact that the ridge geometry used in the tank (particularly fractional height and bottom slope) are significantly different from the actual ridge geometry off Cape Mendocino. There are also errors involved with estimating the various model input parameters. Aside from the errors associated with interpretation of the satellite imagery to measure L_s, L_m, and D_{sw} as discussed earlier, there is error in choosing the appropriate value for h_o. The model also does not account for baroclinic shear in the presence of wind forcing. A final problem is the inability to estimate both the migration rate of the front and the time for the system to reach an equilibrium state from satellite imagery.

In a recent study Narimousa and Maxworthy (1989), hereafter NM89, have fine tuned the 1985 model with better bottom topography, spatially variable wind stress and the addition of variable coastline geometry. The key parameter used was still θ_*, but their revised criteria for instability was changed to about 6.

NM89 also calculated θ_* using a variety of non-synoptic ocean data, and found θ_* to be about 5. We differ from this primarily in our estimate of h_o, which was order 90-100 m during CTZ 87 and CTZ 88, as opposed to 50 m

used by NM89; and in our estimate of u_* (1.0 vs. 1.5 by NM89). These differences produce a θ_* of order 20 and cannot produce eddy shedding. Our alternative method, however using the observed shear (θ_* about 3) would produce eddy shedding in the improved model. We note also that the source of the instability is less clear in NM89, since the effects of bottom topography, coastline geometry, and spatially variable wind stress are combined.

The meaning of θ_* is now examined with the hope of understanding the underlying dynamics causing the observed meandering of the flow. The physical meaning of the parameter θ_* is difficult to assess. The Richardson number only appears in classical studies of the vertical stability in stratified shear flows (e.g., Stern, 1975). The critical value in this case (for Kelvin-Hemholz instability, for example) is Ri = 0.25. Values less than 0.25 are necessary (but not sufficient) for instability, while values greater than 0.25 are definitely stable. Large scale oceanic flows, calculated over tens of meters or more, are virtually always stable when examined in this way. Instability in any case would manifest itself in terms of growing (or breaking) internal waves and enhanced mixing, rather than in any kind of meandering current. The Richardson number simply does not appear in any classical studies of barotropic or baroclinic instability (Stern, 1975; Gill, 1982).

The first part of the formulation, R_D/L_s, looks like an inverse Burger number of sorts (L/R_D), where L is the typical length scale of the jet. Small Burger numbers promote barotropic instability (tall, narrow currents) while larger

Burger numbers favor baroclinic instability (wide, shallow currents). Since θ_* contains a combination of parameters which looks like the inverse of this, and the key criterion is that it be less than 2, we might expect this to favor baroclinic instability. [Barotropic instability seems out in any case, since the length scales and growth rates expected from barotropic instability are much too small (15-20 km) and too fast (8-12 hrs) to explain the observations (Washburn et al., 1988)]. There is a problem however, since L_* is not the width of the jet, which would seem to be the appropriate length scale in this case, but rather the distance of the jet from the coast, which does not seem to have any physical meaning as far as the stability of the jet is concerned. Since θ_* does not contain any information about the aspect ratio of the jet (its width to its depth) or the vorticity gradient across the jet, it would not seem to contain any useful information regarding either barotropic or baroclinic instability. The empirical parameter would appear to be just that, an empirical parameter, which does not contain any useful clues as to the dynamics of the flow.

What, then, are we seeing? The most basic interpretation of the observed flow over a ridge is that the flow must meander to conserve its potential vorticity, much like simple atmospheric flow over a mountain range (Holton, 1972). As the flow approaches the Mendocino Ridge from the north, fluid columns are compressed and must acquire anticyclonic vorticity (turn right, offshore) to conserve their potential vorticity. Just past the ridge, the water deepens a bit again, which would require the columns to move weakly onshore,

and a meandering pattern results. Alternatively, the ridge could simply perturb the flow, which wanders due to baroclinic instability thereafter. Both explanations require that the flow feel the bottom. It is not clear if or how this happens in the tank, since the lower layer flow is in solid body rotation. Such seemingly critical information as the fractional height of the ridge and the horizontal potential vorticity gradient in the water column are also not included in θ_1. In the ocean, there must be a barotropic component of the flow, as yet not well described, which allows the flow to feel the bottom if these possible explanations of the meandering currents off Cape Mendocino are to be of any use.

VI. CONCLUSIONS AND RECOMMENDATIONS

Narimousa and Maxworthy (1985) have produced simulations in a rotating tank that qualitatively appear quite similar to features observed in AVHRR imagery of the ocean off Cape Mendocino and Point Arena. The key factor being investigated was the importance of bottom topography, namely the actual and simulated Mendocino Ridge, in determining the flow field. We have attempted to qualitatively and quantitatively apply this model to the ocean using a quasi-synoptic data set obtained from the region during the Coastal Transition Zone (CTZ) experiment.

The are certain points where the qualitative agreement is quite good. An intense upwelling plume appears at the ridge both in the tank and in the ocean, and features that look like standing waves appear downstream of the ridge. The plume at the ridge becomes unstable in the tank under some circumstances, and eddy shedding occurs. There is weak observational evidence that this also happens in the ocean. Phenomena occurring upstream of the ridge were not investigated.

The quantitative behavior of the fluid was governed in the model by the non-dimensional parameter $\theta_* = g'h_o/fL_ru_*$. This parameter in the NM85 model must be less than 2 for eddy shedding to occur. This condition was relaxed somewhat in a later paper (NM89) to $\theta_* = 6$, when slightly different ridge

geometry, variable coastline geometry, and spatially variable wind stress were included. Quantitative application of the original model equations to oceanic data produced values of θ_* around 20, which means that eddy shedding would not be expected to occur. This formulation also overestimated the observed downstream wavelength (D_{sw}) by a factor of about 3, and gave reasonable agreement for the distance of the head of the plume from the shore at the ridge (L_n, 190 vs. 170 km). We conclude therefore, that the model when applied directly to the ocean does not successfully reproduce the observed features.

New model outputs calculated using the observed shear between the upper and lower ocean, instead of the friction velocity u_* in the upper layer, produced values of θ_* of around 3. This would be marginally "stable" for the original (NM85) model, but would produce eddy shedding in the updated (NM89) version. This formulation underestimates the observed downstream wavelength by a factor of 2, and also slightly underestimates L_n (115 vs. 160 km). When this more realistic formulation for the velocity shear is used with the NM85 model, there is partial success in predicting the behavior of the ocean near Cape Mendocino.

A study of the meaning of the parameter θ_* was also done. This parameter appears to be an empirical one, and does not contain the information essential to evaluating the vorticity, or barotropic or baroclinic instability of the fluid.

APPENDIX

DERIVATION OF MODEL OUTPUT PARAMETERS

The following illustrates the method employed by Narimousa and Maxworthy (1985) to empirically derive the functional relationships between the model output parameters L_n, D_{sw} and θ_*. Eight experiments are run with different values for θ_*. Plots are made of the distance of the head of the plume from the wall versus time. The slope of this plot represents the migration rate of the front, which is in general, a constant. A steady state value of L_n, the steady state distance of the head of the plume from the wall is found graphically from a scatter plot (Figure A.1). The ratio L_n/L_s is plotted logarithmically (Figure A.2) for different values of θ_* and the functional relationship is empirically determined:

$$L_n/L_s = \theta_*^{.25} \qquad \text{(eqn. A.1)}$$

Similar logarithmic plots of D_{sw}/L_s versus θ_* are made (Figure A.3). This yields:

$$D_{sw}/L_s = 0.22\theta_*^{1.15} \qquad \text{(eqn. A.2)}$$

In Figures A.2 and A.3, each data point represents the results of one of the eight experiments performed using different values for θ_*.

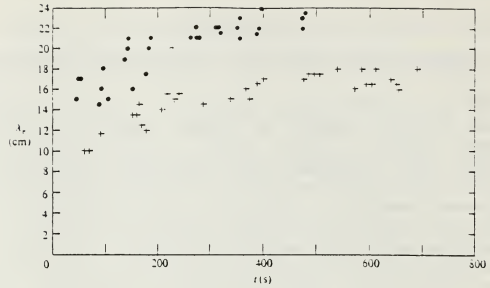

Figure A.1 Scatter plot showing how L_r, the distance of the head of the plume from the tank wall varies with time. (The solid dots represent $\theta_* = 2.03$ and the +'s represent $\theta_* = 36.43$) [From Narimousa and Maxworthy (1985).]

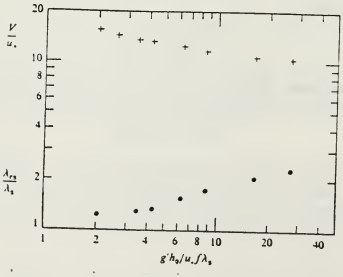

Figure A.2 The bottom data represent variations of L_r/L_s for different values of θ_*. [From Narimousa and Maxworthy (1985).]

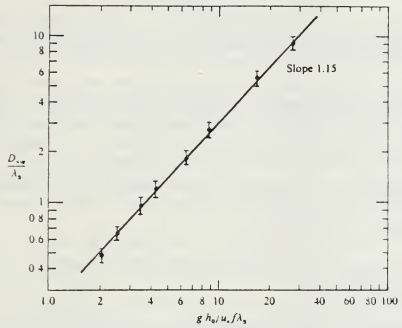

Figure A.3 The variation of D_{sw}/L_s (D_{sw} is the distance of the large standing wave from the maximum plume) with θ_o. [From Narimousa and Maxworthy (1985).]

LIST OF REFERENCES

Allen, J.S., "Models of Wind Driven Currents on the Continental Shelf," *Ann. Rev. Fluid Mech.*, v. 12, pp. 389-432, October 1980.

Barth, J.A., *Stability of a Coastal Upwelling Front,* Ph.D. Dissertation, Woods Hole Oceanographic Institution, Woods Hole, Massachusetts, October 1987.

Batteen, M.L., "Model simulations of a coastal jet and undercurrent in the presence of eddies and jets in the California Current System," The Springer-Verlaglag Lecture Note Volume on *Poleward Flows on Eastern Boundaries* (Neshyba, S., Smith, R.L., Mooers, C.N.K. and Barber, R.A., editors), In press.

Batteen, M.L., Haney, R.L., Tielking, T.A. and Renard P.G., "A numerical study of wind forcing of eddies and jets in the California Current System," *Journal of Marine Research*, v. 47, In press.

Brink, K.H., "The Near Surface Dynamics of Coastal Upwelling," *Prog. Ocean.*, v. 12, pp. 223-257, July 1983.

Brink, K.H., "Upwelling Fronts: Implications and Unknowns," *S. Afr. J. Mar. Sci.*, v. 5, pp. 3-9, January 1987.

Chelton, D.B., "Seasonal Variability of Alongshore Geostrophic Velocity Off Central California," *J. Geophys. Res.*, v. 89, pp. 3473-3486, 20 May 1984.

College of Oceanography, Oregon State University, Data Report 82-8, *Hydrographic data from the first Coastal Ocean Dynamics Experiment R/V Wecoma, Leg 7, July 1-14,* by M. Olivera, W.E. Gilbert, J. Fleischbein, A. Huyer, and R. Schramm, 207 pp., August 1982.

College of Oceanography, Oregon State University, Data Report 141, *CTD Observations in the Coastal Transition Zone Off Northern California, 18 - 27 May 1987,* by R.E. Schramm, J. Fleischbein, R. Marsh, A. Huyer, P.M. Kosro, T. Cowles, and N. Dudek, 192 pp., April 1988.

College of Oceanography, Oregon State University, Data Report 142, *CTD Observations in the Coastal Transition Zone Off Northern California, 9 - 18 June 1987,* by R.E. Schramm, J. Fleischbein, A. Huyer, P.M. Kosro, T. Cowles, and N. Dudek, 228 pp, April 1988.

Crepon, M., Richez, C., and Chartier, M., "Effects of Coastline Geometry on Upwellings," *J. Phys. Oceanogr.*, v. 14, pp. 1365-1382, August 1984.

Gill, A.E., *Atmosphere-Ocean Dynamics*, pp. 29-30, Academic Press, 1982.

Hickey, B.M., "The California Current System - hypothesis and facts," *Prog. in Oceanogr.*, v.8, pp. 191-279, February 1979.

Hickey, B.M., "Alongshore Coherence on the Pacific Northwest Continental Shelf January - April, 1975," *J. Phys. Oceanogr.*, v. 11, pp. 822-835, June 1981.

Holton, J.R., *An Introduction to Dynamic Meteorology*, pp.78-100, Academic Press, 1979.

Huyer, A., "Seasonal Variations in Temperature, Salinity and Density over the Continental Shelf off Oregon," *Limnol. Oceanogr.*, v. 22, pp. 442-453, May 1977.

Huyer, A., "Coastal upwelling in the California current system," *Prog. in Oceanogr.*, v.12, pp. 259-284, February 1983.

Huyer, A., Smith, R.L., and Sobey, E.J.C., "Seasonal Differences in Low - Frequency Current Fluctuations Over the Oregon Continental Shelf," *J. Geophys. Res.*, v. 83, pp. 5077-5089, 20 October 1978.

Huyer, A. and Kosro, P.M., "Mesoscale Surveys Over the Shelf and Slope in the Upwelling Region Near Point Arena, California," *J. Geophys. Res.*, v. 92, pp. 1655-1681, 15 February 1987.

Ikeda, M. and Emery, W.J, "Satellite Observations and Modeling of Meanders in the California Current System off Oregon and Northern California," *J. Phys. Oceanogr.*, v. 14, pp. 1434-1450, September 1984.

Kantha, L.H., Phillips, O.M., amd Azad, R.S., "On turbulent entrainment at a stable density interface," *J. Fluid Mech*, v. 79, pp. 753-768, March 1977.

Kelly,K.A., "The Influence of Winds and Topography on Sea Surface Temperature Patterns Over the Northern California Slope," *J. Geophys. Res.*, v.90, pp. 11,783-11,798, 20 November 1985.

Kosro, P.M. and Huyer, A., "CTD and velocity survey of seaward jets off northern California, July 1981 and 1982," *J. Geophys. Res.*, v.91, pp. 7680-7690, 15 August 1986.

Kosro, P.M., Huyer, A., Cowles, T, Ramp, S.R., Small L., Barber, R.C., Chavez, F., Abbott, M., Strub, P.T., and Jessen, P.F., "The Structure of the Transition Zone Between Coastal Waters and the Open Ocean Off Northern California, Spring 1987," To be submitted to: *J. Geophys. Res.*.

Lentz, S.J., "A Description of the 1981 and 1982 Spring Transitions Over the Northern California Shelf," *J. Geophys. Res.*, v. 92, pp. 1545-1567, 15 February 1987.

McCreary, J.P., Kundu, P.K., and Chao, S.Y., "On the Dynamics of the California Current System," *Journal of Marine Research*, v. 45, pp. 1-32, January 1987.

Narimousa, S. and Maxworthy, T., "Two Layer Model of Shear Driven Coastal Upwelling in the Presence of Bottom Topography," *J. Fluid Mech.*, v. 159, pp. 503-531, October 1985.

Narimousa, S. and Maxworthy, T., "On the Effects of Coastline Perturbations on Coastal Currents and Fronts," *J. Phys. Oceanogr.* v. 17, pp. 1296-1303, August 1987.

Narimousa, S. and Maxworthy, T., "Application of a Laboratory Model to the Interpretation of Satellite and Field Observations of Coastal Upwelling," *Dynamics of Atmospheres and Oceans*, v.13, May 1989.

Niiler, P.P. and Brink, K.H., Telephone Conversation between K.H. Brink, Woods Hole Oceanographic Institution and W.C. Fasciano, Naval Postgraduate School, 13 March 1989.

Office of Naval Research, *Coastal Transition Zone Workshop Report*, by K.H. Brink and E.O. Hartwig, 69 pp. May 1985.

Peffley, M.B. and O'Brien, J.J., "A Three Dimensional Simulation of Coastal Upwelling Off Oregon," *J. Phys. Oceanogr.*, v. 6, pp. 164-180, February 1976.

Preller, R. and O'Brien, J.J., "The influence of bottom topography on upwelling off Peru," *J. Phys. Oceanogr.*, v. 10, pp. 1377-1398, May 1980.

Reid, J.L. and Schwartzlose, R.A., "Direct Measurements of the Davidson Current Off Central California," *J. Geophys. Res.*, v. 67, pp. 2491-2497, June 1962.

Reinecker, M.M., Mooers, C.N.K., and Robinson, A.R., "Dynamical Interpolation and Forecast of the Evolution of Mesoscale Features off Northern California," *J. Phys. Oceanogr.*, v. 17, pp. 1189-1213, August 1987.

School of Oceanography, Oregon State University, Data Report 90, *CTD Observations Off Oregon and California, 5-17 February 1981*, by J. Fleischbein, W.E. Gilbert, R. Schramm, and A. Huyer, 122 pp., March 1982.

Simpson, J.J., Koblinsky, C.J., Pelaez, J., Haury, L.R., and Wiesenhahn, "Temperature - Plant Pigment - Optical Relations in a Recurrent Offshore Mesoscale Eddy Near Point Conception, California," *J. Geophys. Res.*, v. 91, pp. 12, 919-12, 936, 15 November 1986.

Stern, M.E., *Ocean Circulation Physics*, pp. 135-168, Academic Press, 1975.

Strub, P.T., Allen, J.S., Huyer, A., and Smith, R.L., "Large Scale Structure of the Spring Transition in the Coastal Ocean Off Western North America," *J. Geophys. Res.*, v. 92, pp. 1527-1544, 15 February 1987.

Sverdrup, H.U., Johnson, M.W., and Fleming, R.H., *The Oceans: Their Physics, Chemistry and General Biology*, p. 605-761, Prentice Hall, 1942.

The CTZ Group, " The Coastal Transition Zone Program," *EOS Trans. AGU*, v. 69, No. 27, pp. 1-4, 5 July 1988.

Tibby, R.B., "The Water Masses of the West Coast of North America," *Journal of Marine Research*, v. 4, pp. 112-121, February 1941.

University of Hawaii, Hawaii Inst. of Geophysics Report 74-5, *The Dynamic Topography of the Pacific Ocean and its Fluctuations*, by K. Wyrtki, pp. 1-37, May 1974.

U.S. Department of Commerce, National Oceanic and Atmospheric Administration NOAA Technical Report NMFS SSRF-714, *Wind stress and wind stress curl over the California Current*, by C.S. Nelson, 87 pp., 1977.

Washburn, L., and Armi, L., "Observations on Frontal Instabilities on an Upwelling Filament," *J. Phys. Oceanogr.*, v. 18, pp. 1075-1092, August 1988.

Watts, R.D. and Johns W.E., "Gulf stream Meanders: Observations on Propagation and Growth," *J. Geophys. Res.*, v.87, pp. 9467-9476, 20 November 1982.

Winant, C.D., Beardsley, R.C., and Davis, R.E., "Moored Wind, Temperature and Current Observations Made During CODE - 1 and CODE - 2 Over the Northern California Continental Shelf and Upper Slope," *J. Geophys. Res.*, v. 92, pp. 1569-1604, 15 February 1987.

Wyatt, B., Burt, W.V., and Pattullo, J.G., "Surface Currents Off Oregon as Determined from Drift Bottle Returns," *J. Phys. Oceanogr.*, v. 2, pp. 286,293, July 1972.

INITIAL DISTRIBUTION LIST

		No. Copies
1.	Defense Technical Information Center Cameron Station Alexandria VA 22304-6145	2
2.	Library, Code 0142 Naval Postgraduate School Monterey, CA 93943	2
3.	Director, Naval Oceanography Division Naval Observatory 34th and Massachusetts Avenue, NW Washington, DC 20390	1
4.	Commander Naval Oceanography Command NSTL Station, MS 39529	1
5.	Commanding Officer Naval Oceanographic Office NSTL Station Bay St. Louis, MS 39522	1
6.	Commanding Officer Fleet Numerical Oceanography Center Monterey, CA 93943	1
7.	Commanding Officer Naval Ocean Research and Development Activity NSTL Station, Bay St. Louis, MS 39529	1
8.	Commanding Officer Naval Environmental Prediction Research Facility Monterey, CA 93943	1

9.	Chairman, Code 68Co Department of Oceanography Naval Postgraduate School Monterey, CA 93943	1
10.	Professor S.R. Ramp, Code 68Ra Department of Oceanography Naval Postgraduate School Monterey, CA 93943	1
11.	Professor M.L. Batteen, Code 68Bv Department of Oceanography Naval Postgraduate School Monterey, CA 93943	1
12.	Professor R.L. Haney, Code 63Hy Department of Meteorology Naval Postgraduate School Monterey, CA 93943	1
13.	LCDR William C. Fasciano Fleet Numerical Oceanography Center Monterey, CA 93943	5
14.	Library John Carroll University University Heights, OH 44118	1
15.	Library Humboldt State University Arcata, CA 95521	1
16.	Library College of Oceanography Oregon State University Corvallis, OR 97331	1

17.	Professor R.L. Smith College of Oceanography Oregon State University Corvallis, OR 97331	1
18.	Professor A. Huyer College of Oceanography Oregon State University Corvallis, OR 97331	1
19.	Professor P.M. Kosro College of Oceanography Oregon State University Corvallis, OR 97331	1
20.	Library College of the Redwoods Eureka, CA 95501	1
21.	Office of Naval Research Code 1122CS 800 North Quincy Street Arlington, VA 22217 Attn: Dr. Tom Kinder	1
22.	Professor T.P. Stanton, Code 68St Department of Oceanography Naval Postgraduate School Monterey, CA 93943	1

Thesis
F2372 Fasciano
c.1 Meandering of the coastal upwelling jet near Cape Mendocino, California.

15 AUG 90 35547

Thesis
F2372 Fasciano
c.1 Meandering of the coastal upwelling jet near Cape Mendocino, California.

thesis2372
Meandering of the coastal upwelling jet
3 2768 000 82889 1
DUDLEY KNOX LIBRARY